





1998

# Airfoil Geometry and Flow Compressibility Effects on Wing and Blade Flutter

Jones, K.D.

# AIAA−98−0517
# AIRFOIL GEOMETRY AND COMPRESSIBILITY EFFECTS ON WING AND BLADE FLUTTER

K.D.Jones and M.F.Platzer
Naval Postgraduate School
Monterey, CA

**36th Aerospace Sciences Meeting & Exhibit**
January 12−15,1998 / Reno, NV

# AIRFOIL GEOMETRY AND FLOW COMPRESSIBILITY EFFECTS ON WING AND BLADE FLUTTER

**K. D. Jones[†] and M. F. Platzer[‡]**

Naval Postgraduate School
Monterey, California

## ABSTRACT

An unsteady, two-dimensional, incompressible potential-flow solver and an unsteady, two-dimensional, compressible Euler/Navier-Stokes flow solver are coupled with a two-degree-of-freedom structural model for the time-domain computation of aeroelastic response. Comparisons are made between results from the two flow solvers and with flutter boundary predictions of linear theory. Presented results demonstrate similar destabilizing effects for both increasing airfoil thickness and increasing Mach number. More importantly, it is shown that linear theory yields un-conservative flutter-velocity predictions. While linear theory predicts that single-degree-of-freedom (pitching) flutter cannot occur except with an unrealistically high sectional moment of inertia, it is shown here that thicker airfoils in compressible flows may easily achieve single-degree-of-freedom flutter under realistic conditions.

## NOMENCLATURE

$a_\infty$ = freestream speed of sound
$c$ = chord length
$C_l$ = lift coefficient per unit span
$C_m$ = pitching moment coefficient per unit span
$f$ = frequency in Hertz
$h$ = bending displacement (positive downward)
$I_\alpha$ = moment of inertia about $x_p$ per unit span
$k$ = reduced frequency, $2\pi c/U_\infty$
$k_\alpha$ = reduced natural pitching frequency
$k_h$ = reduced natural plunging frequency
$K_h$ = spring constant for plunging
$K_\alpha$ = spring constant for pitching
$L$ = lift per unit span
$m$ = mass of the wing per unit span
$M$ = pitching moment per unit span
$\mathbf{M}_\infty$ = freestream Mach number
$S_\alpha$ = static moment, $x_\alpha m$
$t$ = time
$\mathbf{V_F}$ = reduced flutter velocity, $U_\infty/(c\omega_\alpha) = 1/k_\alpha$
$U_\infty$ = freestream velocity magnitude
$x_p$ = leading edge to elastic axis distance
$x_\alpha$ = elastic axis to center of mass distance
$\alpha$ = angle of attack
$\omega_h$ = uncoupled natural bending freq., $\sqrt{K_h/m}$
$\omega_\alpha$ = uncoupled natural torsional freq., $\sqrt{K_\alpha/I_\alpha}$
$\rho_\infty$ = freestream density
$\tau$ = nondimensional time, $tU_\infty/c$
$(\dot{})$ = differentiation with respect to $t$
$(\,)'$ = differentiation with respect to $\tau$

## INTRODUCTION

Aerodynamically driven instability of flexible aircraft components has been a topic of considerable interest to the engineering community for the greater part of this century. Applications for such research are numerous including the design of aircraft wings, empennages, helicopter and propeller blades, turbomachinery and even earth-bound structures. The Tacoma Narrows suspension bridge, destroyed back in 1940 after many hours of divergent, wind-driven oscillations, is a classic example of this.

In 1934 Theodorsen[1] provided the first compact theoretical analysis of wing and wing/aileron flutter. Theodorsen's linearized theory modeled the airfoil as a flat-plate and the wake as a non-deforming, semi-infinite sheet of vorticity trailing the airfoil. Stability analysis was performed in the frequency-domain by means of the tabulated Theodorsen lift deficiency function. Theodorsen's formulations have been applied to many interesting aerodynamics problems including wing and aileron flutter by Theodorsen and Garrick,[2] flapping-wing propulsion by Garrick[3] and rotary-wing aerodynamics by Loewy,[4] to name just a few.

Before Theodorsen's work it was thought that flutter required a minimum of two degrees-of-freedom. However, Theodorsen demonstrated that single-degree-of-freedom (SDOF) flutter was possible, but only at a very low reduced frequency, corresponding to a very high flutter velocity. Additionally, Smilg pointed out

---

[†] Research Assistant Prof., Senior Member, AIAA

[‡] Professor, Associate Fellow, AIAA

that even though SDOF flutter was theoretically possible, it was of little practical interest, since linear theory required the sectional moment of inertia, $I_\alpha$, to be several orders of magnitude higher than is typically found on aircraft.[5]

In 1951, Runyan showed that flow compressibility lowered the SDOF flutter reduced velocity substantially in high subsonic and low supersonic flow.[6] This is discussed in some detail in Bisplinghoff et al.[7] They point out that while the minimum inertial parameter required for flutter is still too large for an airfoil alone, it is reasonable for a complete aircraft. This remark is of little concern, however, as it is unlikely that a free flying complete aircraft would undergo SDOF motions. Even if the aircraft was treated as a rigid body, there would almost certainly be some translational motion of the center of gravity.

Recently, due to a rapid increase in available computational power, a host of unsteady Computational Fluid Dynamics (CFD) algorithms have been developed. There is a large variation in the applicability and computational efficiency of these algorithms. On one end of the scale are very fast algorithms solving for potential flows, approximating the fluid as incompressible, inviscid and irrotational. On the other end of the scale are algorithms that solve the Navier-Stokes equations.

While all of the classical numerical studies cited above perform stability analysis in the frequency domain, the development of these more general, time-stepping algorithms suggests the use of time-domain aeroelastic algorithms, coupling fluids and structural analysis in a time-stepping code. Indeed, numerous studies of this nature have been performed, but few address some of the basic issues that arise from this type of analysis.

In the present study a potential-flow solver and an Euler/Navier-Stokes solver are coupled with a two-degree-of-freedom (TDOF) structural model for the time-domain analysis of aeroelasticity. By limiting the analysis to a relatively simple two-dimensional configuration comparisons can be made with linear theory and between the two flow solvers to accurately assess the influences of wake non-linearities, airfoil geometry and flow compressibility.

Time constraints, unfortunately, have limited this study to SDOF-pitching instabilities, and only inviscid analysis was performed. For the low angles-of-attack considered here, the flows should be attached and the effect of viscosity would be very small. Furthermore, the compressible simulations are limited to subsonic and low transonic speeds such that shock/boundary-layer-interaction effects would be negligible.

## NUMERICAL METHODS

Aeroelasticity is a multi-disciplinary subject combining aerodynamics and structural dynamics. The methods used in the present study for each discipline are outlined in the sections below.

### AERODYNAMICS

Flow solutions are computed using two unsteady algorithms; a potential-flow solver for incompressible flows and an Euler/Navier-Stokes code for compressible flows. Both codes were previously developed and are well documented in the literature, but brief descriptions of the methods are included here for clarity.

**Incompressible Flow Solutions** Incompressible flow solutions are computed using an unsteady potential-flow, or panel method. The panel code, developed by Teng,[8] has been well documented in past publications (Refs. 9-14) with aeroelastic coupling developed and tested by Jones and Platzer.[15]

The basic, steady panel code follows the approach of Hess and Smith,[16] where the airfoil is approximated by a number of panels (typically 100-400), each with a unique, distributed source strength and all with a constant distributed vorticity strength. For $n$ panels there are $n$ unknown source strengths, $q_j$, and an unknown vorticity strength, $\gamma$. Boundary conditions include flow tangency at the midpoint of the $n$ panels and the Kutta condition which postulates that the pressure on the upper and lower surfaces of the airfoil at the trailing edge must be equal.

The unsteady panel code adopts the procedure of Basu and Hancock,[17] where a wake panel is attached to the trailing edge through which vorticity is shed into the flow. The Helmholtz theorem states that the bound vorticity in a flow remains constant, thus a change in circulation about the airfoil must result in the release of vorticity into the wake equal in magnitude and opposite in direction. Numerically this is given by

$$\Delta_k(\gamma_W)_k + \Gamma_k = \Gamma_{k-1} \tag{1}$$

where $\Delta$ is the wake panel length, $\gamma_W$ is the distributed vorticity strength on the wake panel and $\Gamma$ is the circulation about the airfoil, and where the subscript $k$ indicates the current time step, and $k-1$ indicates the previous time step.

The wake panel introduces two additional unknowns; the wake panel length and its orientation, $\theta_k$. Thus, two additional conditions must be specified for closure;

1. The wake panel is oriented in the direction of the local resultant velocity at the panel midpoint.

2. The length of the wake panel is proportional to the magnitude of the local resultant velocity at the panel midpoint and the time-step size.

The essential elements of this scheme are summarized in Fig. 1.

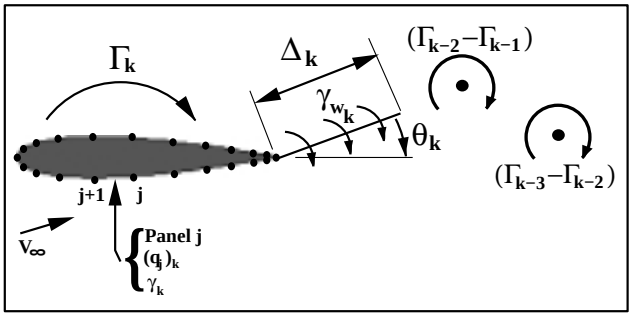


**Fig. 1.** Schematic of the panel code wake model.

At the end of each time step the vorticity contained in the wake panel is concentrated into a point vortex which is shed into the wake and convected downstream with the flow, influencing and being influenced by the other shed vortices and the airfoil. Note, implementation of this approach requires an iterative scheme, since the velocity direction and magnitude used to define the wake panel are not initially known. Note also that this wake model is nonlinear.

**Compressible Flow Solutions** The unsteady, compressible Euler/Navier-Stokes algorithm solves the strong conservation-law form of the two-dimensional, thin-layer Navier-Stokes equations in a curvilinear coordinate system $(\xi, \zeta)$. The governing equations are given in vector form by

$$\partial_t \hat{\mathbf{Q}} + \partial_\xi \hat{\mathbf{F}} + \partial_\zeta \hat{\mathbf{G}} = Re^{-1} \partial_\zeta \hat{\mathbf{S}} \tag{2}$$

where $\hat{\mathbf{Q}}$ is the vector of conservative variables,

$$\hat{\mathbf{Q}} = \frac{1}{J} \begin{Bmatrix} \rho \\ \rho u \\ \rho w \\ e \end{Bmatrix}, \tag{3}$$

$\hat{\mathbf{F}}$ and $\hat{\mathbf{G}}$ are the inviscid flux vectors,

$$\hat{\mathbf{F}} = \frac{1}{J} \begin{Bmatrix} \rho U \\ \rho u U + \xi_x p \\ \rho w U + \xi_z p \\ (e+p)U - \xi_t p \end{Bmatrix}, \tag{4}$$

$$\hat{\mathbf{G}} = \frac{1}{J} \begin{Bmatrix} \rho W \\ \rho u W + \zeta_x p \\ \rho w W + \zeta_z p \\ (e+p)W - \zeta_t p \end{Bmatrix} \tag{5}$$

and $\hat{\mathbf{S}}$ is the thin-layer approximation of the viscous fluxes in the $\zeta$ direction (normal to the airfoil surface),

$$\hat{\mathbf{S}} = \frac{1}{J} \begin{Bmatrix} 0 \\ \mu m_1 u_\zeta + (\mu/3) m_2 \zeta_x \\ \mu m_1 w_\zeta + (\mu/3) m_2 \zeta_z \\ \mu m_1 m_3 + (\mu/3) m_2 m_4 \end{Bmatrix}, \tag{6}$$

where

$$m_1 = \zeta_x^2 + \zeta_z^2, \tag{7}$$

$$m_2 = \zeta_x u_\zeta + \zeta_z w_\zeta, \tag{8}$$

$$m_3 = (u^2 + w^2)/2 + (\gamma - 1)^{-1} Pr^{-1} \partial_\zeta (a^2) \tag{9}$$

and

$$m_4 = \zeta_x u + \zeta_z w. \tag{10}$$

The terms $U$ and $W$ are the contravariant velocity components given by

$$U = u\xi_x + w\xi_z + \xi_t \tag{11}$$

and

$$W = u\zeta_x + w\zeta_z + \zeta_t \tag{12}$$

and $J$ is the metric Jacobian, where

$$J^{-1} = x_\xi z_\zeta - x_\zeta z_\xi \ . \tag{13}$$

Pressure is related to the other variables through the equation of state for an ideal gas

$$p = (\gamma - 1)\Big[e - \rho(u^2 + w^2)/2\Big] \tag{14}$$

Nondimensionalization of Eqs. (2-14) is performed using $c$ as the reference length, $a_\infty$ as the reference velocity, $c/a_\infty$ as the reference time, $\rho_\infty$ as the reference density and $\rho_\infty a_\infty^2$ as the reference energy. The form of the equations does not change after the nondimensionalization. Note, this nondimensionalization differs from the panel code; using $a_\infty$ as the reference velocity here. This provides a different time scale and a different definition for the reduced frequency; however, for clarity, the presented results have been rescaled using the time and reduced frequency definitions of the panel code and shown in the nomenclature.

For Euler solutions the viscous terms on the RHS are set to zero, and flow tangency boundary conditions are applied at the surface. For Navier-Stokes solutions the no-slip condition is applied at the surface. Density and pressure are extrapolated to the surface for both Euler and Navier-Stokes solutions, and for unsteady motions the flow-tangency and no-slip conditions are modified to include the local motion of the surface.

In the present study the effect of flow compressibility is of interest, therefore, only Euler (inviscid)

solutions are computed. In future studies viscous calculations may be performed to investigate the effect of shock/boundary-layer interactions and flow separation on the flutter response.

The time-integration is performed using the upwind biased, factorized, iterative, implicit scheme of Chakravarthy and Osher,[18] given by

$$\begin{aligned}
&\left[I+h_\xi\left(\nabla_\xi \hat{A}^+_{i,k}+\Delta_\xi \hat{A}^-_{i,k}\right)\right]^p \\
&\quad\times\left[I+h_\zeta\left(\nabla_\zeta \hat{B}^+_{i,k}+\Delta_\zeta \hat{B}^-_{i,k}-Re^{-1}\delta_\zeta \hat{M}_{i,k}\right)\right]^p \\
&\quad\times\left(\hat{Q}^{p+1}_{i,k}-\hat{Q}^p_{i,k}\right) \\
&= -\Bigg[\left(\hat{Q}^p_{i,k}-\hat{Q}^n_{i,k}\right) \\
&\quad+h_\xi\left(\hat{F}^p_{i+1/2,k}-\hat{F}^p_{i-1/2,k}\right) \\
&\quad+h_\zeta\left(\hat{G}^p_{i,k+1/2}-\hat{G}^p_{i,k-1/2}\right) \\
&\quad-Re^{-1}h_\zeta\left(\hat{S}^p_{i,k+1/2}-\hat{S}^p_{i,k-1/2}\right)\Bigg]
\end{aligned} \tag{15}$$

In Eq. (15), $h_\xi = \Delta\tau/\Delta\xi$ etc., $\hat{A}^\pm = \partial\hat{F}/\partial\hat{Q}$ etc. are the flux Jacobian matrices and $\nabla$, $\Delta$ and $\delta$ are the forward, backward and central difference operators, respectively. The quantities $\hat{F}_{i+1/2,k}$, $\hat{G}_{i,k+1/2}$ and $\hat{S}_{i,k+1/2}$ are numerical fluxes. The superscript $(\cdot)^n$ denotes the time step, and the superscript $(\cdot)^p$ refers to Newton subiterations within each time step.

The inviscid fluxes, $\hat{F}$ and $\hat{G}$, are evaluated using Osher's third-order upwinding scheme.[19] For the linearization of the left-hand side of Eq. (15) the flux Jacobian matrices, $A$ and $B$, are evaluated by the Steger-Warming flux-vector splitting.[20] The viscous fluxes are computed with second-order central differences.

Time accuracy is improved by performing Newton subiterations to convergence at each step. These subiterations minimize the linearization and factorization errors and help drive the left-hand side of Eq. (15) to zero at each time step. Experiments by the present authors found that larger CFL numbers (i.e., a larger time step) could be used if the number of Newton iterations was increased. The optimum seemed to depend on the grid topology and flow conditions, but the best computational performance seemed to occur with 4 to 5 sub-iterations on coarse grids (Euler simulations), and 2 to 3 sub-iterations on fine grids (Navier-Stokes simulations). The Navier-Stokes solver has been tested extensively in a variety of unsteady subsonic, transonic and supersonic studies (Refs. 21-23).

A typical computational grid used for the Euler simulations is shown in Fig. 2, with a detailed view of the surface in Fig. 3. The grid shown, for a NACA0012 airfoil section, has $201 \times 41$ points, with an initial wall spacing of 0.002, 31 points in the wake and a farfield boundary 10 chordlengths from the surface.

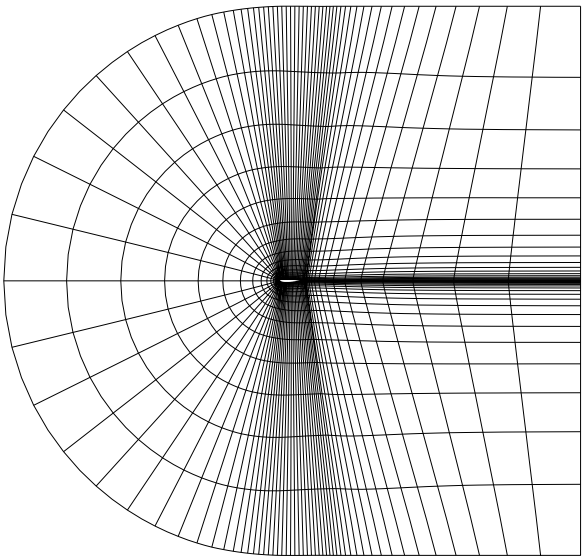

**Fig. 2.** Euler grid ($201 \times 41$, every-other line shown).

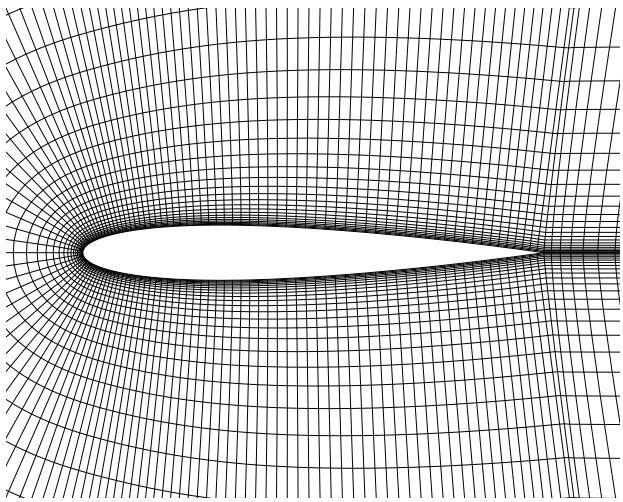

**Fig. 3.** Euler grid surface detail.

The Euler solutions are actually quite sensitive to the initial wall spacing and orthogonality near the wall. While relaxed surface spacing and normals result in almost no change in the lift, they result in a slight shift in the moment and the unsteady phasing of the moment. The phase of the moment is the key to SDOF-pitching flutter, thus its accurate computation is essential.

A number of validation experiments were performed to verify the quality of the grids. The grid density was increased to $301 \times 61$, resulting in virtually no variation in the predicted flutter frequency. Additionally, the initial wall spacing was reduced to 0.001,

again with negligible influence on the results. (Note, for the NACA 0006 airfoil section, an initial spacing of 0.0005 was required near the leading edge.)

Experimental results with the panel code demonstrated that several initial, or start-up, oscillation cycles were required before an accurate measurement of the flutter response could be obtained. At the low frequencies involved in this study, several cycles corresponds to a computed wake length on the order of 100 chordlengths. A computational domain of this magnitude is not realistically feasible for the Euler code. However, the effect of the wake resolution was investigated, both by increasing the wake point density and by doubling the extension of the computational domain in the streamwise direction. Fortunately, predicted flutter frequencies only varied by approximately 0.1% for the extended, high density computational domain, a variation that was deemed tolerable for the present study.

## STRUCTURAL DYNAMICS

Structural modeling is facilitated using a TDOF spring/mass system (Fig. 4) to simulate the bending and twisting of a wing.

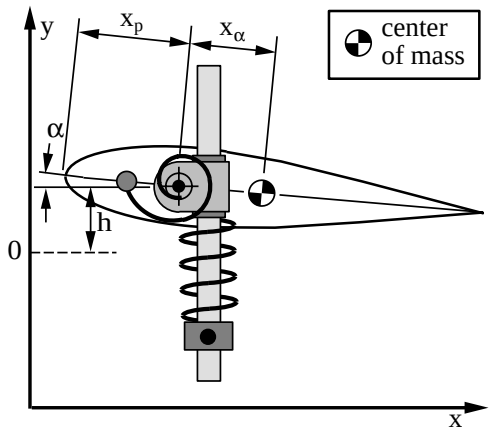


**Fig. 4.** Schematic of the spring/mass system.

The equations governing this motion are

$$m\ddot{h} + S_\alpha \ddot{\alpha} + m\omega_h^2 h = -L \tag{16}$$

and

$$S_\alpha \ddot{h} + I_\alpha \ddot{\alpha} + I_\alpha \omega_\alpha^2 \alpha = M \ , \tag{17}$$

where the dots denote differentiation with respect to time. Note, no structural damping is considered here.

For the panel code the system is nondimensionalized using $c$ as the reference length, $V_\infty$ as the reference velocity, $c/V_\infty$ as the reference time and $c^2\pi\rho_\infty/4$ as the reference mass. Rewriting the system in matrix notation, one obtains

$$[\mathbf{M}]\{X\}'' + [\mathbf{k}]\{X\} = \{F\} \tag{18}$$

where

$$[\mathbf{M}] = \begin{bmatrix} m & S_\alpha \\ S_\alpha & I_\alpha \end{bmatrix}, \ [\mathbf{k}] = \begin{bmatrix} mk_h^2 & 0 \\ 0 & I_\alpha k_\alpha^2 \end{bmatrix},$$

$$\{X\} = \begin{Bmatrix} h \\ \alpha \end{Bmatrix} \ \text{ and } \{F\} = \frac{2}{\pi} \begin{Bmatrix} -C_l \\ C_m \end{Bmatrix},$$

and where the primes denote differentiation with respect to nondimensional time, $\tau$.

Equation (18) is a system of two, coupled, second-order, nonlinear, differential equations; coupled through the terms containing $S_\alpha$ and the dependence of $C_l$ and $C_m$ on $h$ and $\alpha$, and nonlinear through the nonlinearity of $C_l$ and $C_m$.

Nondimensionalization for the Euler/Navier-Stokes code is performed similarly, but the reference velocity is the freestream speed of sound, $a_\infty$, and the reference time is then $c/a_\infty$. The resulting system of equations is the same as Eq. (18) except for the RHS vector $\{F\}$ which becomes

$$\{F\} = \frac{2}{\pi}\mathbf{M}_\infty^2 \begin{Bmatrix} -C_l \\ C_m \end{Bmatrix}. \tag{19}$$

Note that $k_h$ and $k_\alpha$ appearing in the matrix $[\mathbf{k}]$ are reduced natural frequencies based on the freestream speed of sound, but presented results convert them to the conventional definition, based on freestream velocity, to be consistent with the incompressible analysis.

Simulations with a SDOF are performed by setting $S_\alpha = 0$ and either $m = \infty$ and $\omega_h = 0$ or $I_\alpha = \infty$ and $\omega_\alpha = 0$ for pitching-only or plunging-only motions, respectively.

Equation (18) is advanced in time by inverting the system, yielding

$$\{X\}'' = [\mathbf{M}]^{-1}\{F\} - [\mathbf{M}]^{-1}[\mathbf{k}]\{X\} \ , \tag{20}$$

then rewriting the result as a system of two coupled, first-order equations

$$\begin{aligned} \{X\}' &= \{Y\} \\ \{Y\}' &= [\mathbf{M}]^{-1}\{F\} - [\mathbf{M}]^{-1}[\mathbf{k}]\{X\} \ , \end{aligned} \tag{21}$$

and, finally, integration is performed using an Euler or a 4th-order Runge-Kutta scheme. The panel code uses relatively large time steps, and thus requires the 4th-order integration scheme for sufficient accuracy, but the stability requirements of the Euler/Navier-Stokes code are such that time-steps are small enough to achieve sufficient accuracy with a 1st-order Euler integration scheme. Panel solutions typically have about 120 steps per cycle, and the Euler simulations have

between 600 and 6000 steps per cycle, dependent on the stability limitations of the Euler code.

## RESULTS

In the present study only SDOF simulations are performed, reserving the TDOF case for a future study. In the first part, the effect of airfoil thickness is investigated in incompressible flow, with comparisons to linear theory, and in the second part the effect of flow compressibility is investigated for several airfoils with comparisons to the incompressible, panel-code solutions and linear theory.

Aeroelastic simulations are produced by computing a steady flow solution at an 0.5 degree angle of attack, and releasing the airfoil at the start of the unsteady solution. With the spring-neutral set at 0 degrees, the static imbalance causes the airfoil to pitch, and the gain or loss of mechanical energy is used to measure the stability of the airfoil. The flutter condition is marked by a constant mechanical energy.

## GEOMETRY EFFECTS

In the literature it is often stated that for incompressible flow SDOF flutter in pitching (SDOF plunging is always stable) is only of academic interest, since linear theory does not predict flutter except with an airfoil sectional moment of inertia far exceeding realistic values (e.g., Refs. 5 and 7). The panel code is used here to investigate the effect of airfoil thickness on the predicted flutter boundaries. This was done to some degree in Ref. 15, with the relevant results presented there in Fig. 10, and repeated here in Fig. 5. The results are for several symmetrical NACA airfoils pivoting about their leading edges.

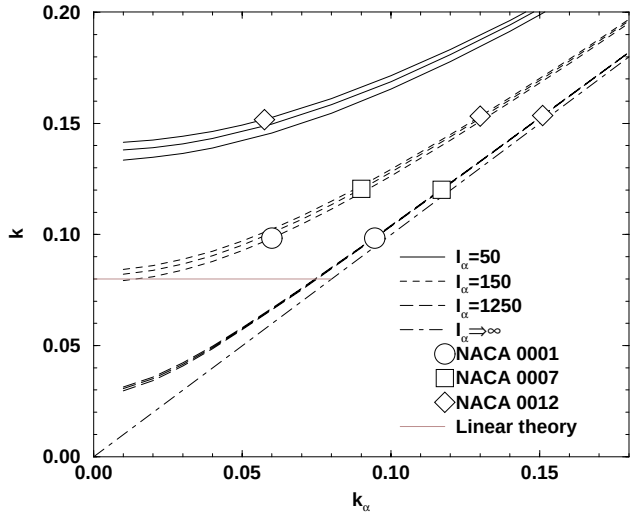


**Fig. 5.** Frequency response and flutter boundaries.

In Fig. 5, the three sets of three curves plot the resultant oscillation frequency, $k$, as a function of the undamped natural frequency, $k_\alpha$, for three airfoils and three inertial parameters. In each grouping of three lines, the upper line corresponds to a NACA0012 airfoil, the middle line to a NACA 0007 airfoil and the lower line to a NACA 0001 airfoil. The circle, square and diamond symbols denote the point along the curves where flutter occurs for the NACA 0001, 0007 and 0012 airfoils, respectively. Important features to note from Fig. 5 are that the flutter frequency is independent of the inertial parameter, in accordance with linear theory, the frequency response is only slightly dependent on the airfoil thickness, but the flutter frequencies are highly dependent on the thickness, reducing both the flutter velocity and the minimum required inertial parameter. As the airfoil thickness is reduced, the flutter frequency approaches that predicted by linear theory, although not asymptotically, a fact that requires further attention in future studies.

In Fig. 6 the nondimensional flutter velocity, $V_F$, is plotted for a range of airfoils as a function of the nondimensional inertial parameter, $I_\alpha$. Clearly airfoil thickness is a destabilizing feature providing much lower flutter velocities and at much more realistic values of $I_\alpha$.

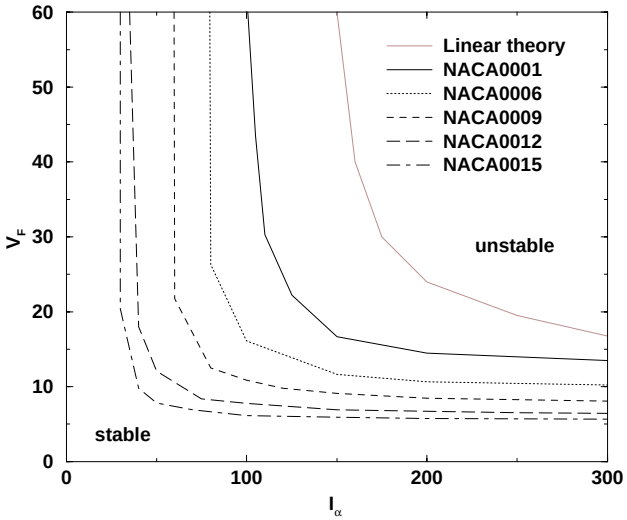


**Fig. 6.** Flutter velocity versus thickness and $I_\alpha$.

The effect of the elastic axis location was investigated in Refs. 5 and 6 using linear theory. In Fig. 7 the linear results given in Ref. 24 (originally extracted from Refs. 5 and 6) are plotted along with results from the panel code for NACA0006 and NACA0015 airfoil sections. Note the much higher reduced flutter frequencies (corresponding to much lower reduced flutter velocities) for the thicker sections. Also note that two sets of data points for the NACA0006 and four sets

for the NACA0015, corresponding to different values of $I_\alpha$, as indicated in the figure legends, are included, and are essentially coincident. Recall from Fig. 5 that the flutter frequency was shown to be independent of $I_\alpha$. In Fig. 7, this is shown to be true for all elastic axis locations.

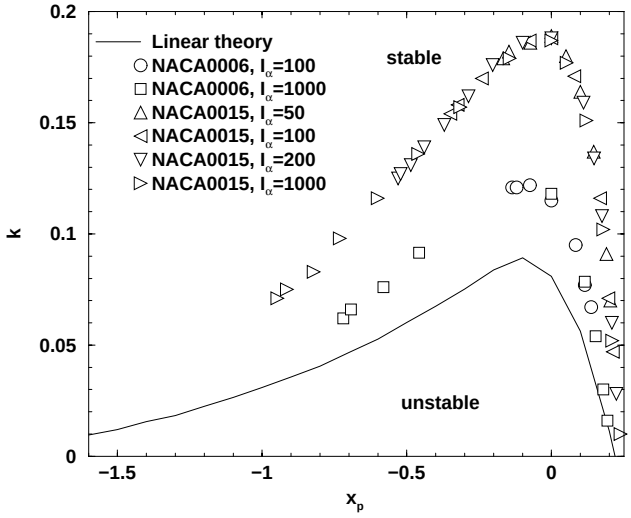


**Fig. 7.** Incompressible flutter-instability regions.

Similar data are shown in Figs. 8 and 9, for the NACA0006 and NACA0015 airfoils, respectively. However, both the values of $k_\alpha$ and $k$ are included in these figures. Values of $k_\alpha$ for different values of $I_\alpha$ are plotted by the lines (with each line-type associated with a given value of $I_\alpha$, as indicated in the figure legends) and the values of $k$ are denoted by the stars. One very important feature shown in Figs. 8 and 9 is that elastic-axis locations that result in flutter become quite limited as $I_\alpha$ is reduced.

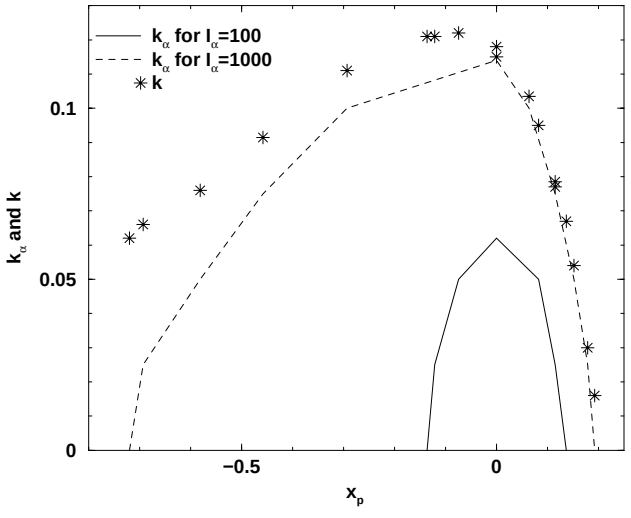


**Fig. 8.** Region of flutter-instability for a NACA0006.

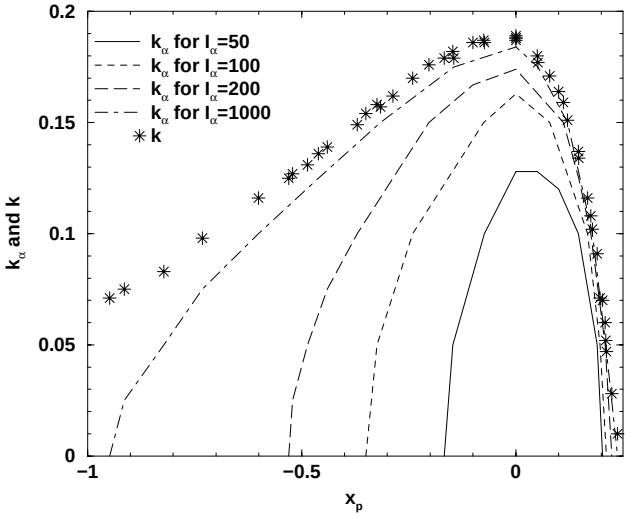


**Fig. 9.** Region of flutter-instability for a NACA0015.

## COMPRESSIBILITY EFFECTS

Results from the compressible Euler code are compared with incompressible and compressible linear theory (for a flat plate) and with the panel code (for airfoils of finite thickness and incompressible flow) to investigate the effects of flow compressibility. As previously mentioned, the flow is restricted to subsonic and very low transonic speeds to prevent the formation of strong shocks. For the data presented here the Mach number is limited to a maximum value of 0.7, and for the small angle of attack range of interest here ($\alpha \approx \pm 0.5$ degrees), a very weak shock is visible on the suction side of a NACA0015 at a static angle of attack of 0.5 degrees, as shown in Fig. 10. The contour lines denote Mach intervals of 0.05, with the grey (or dotted) contour indicating the sonic line.

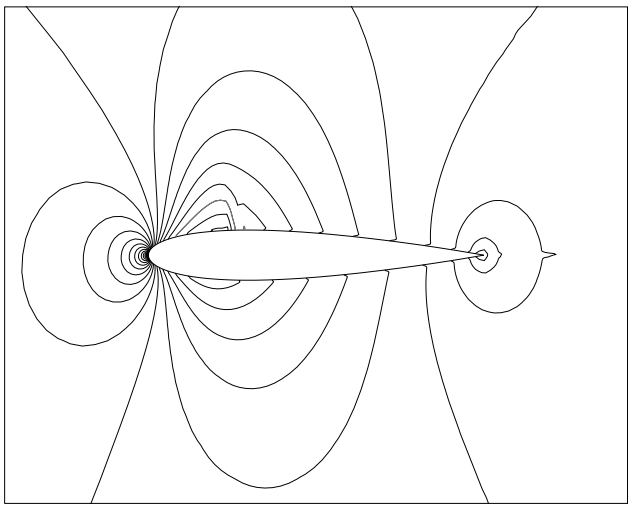

**Fig. 10.** Steady Mach contours; $M_\infty = 0.7$, $\alpha = 0.5°$.

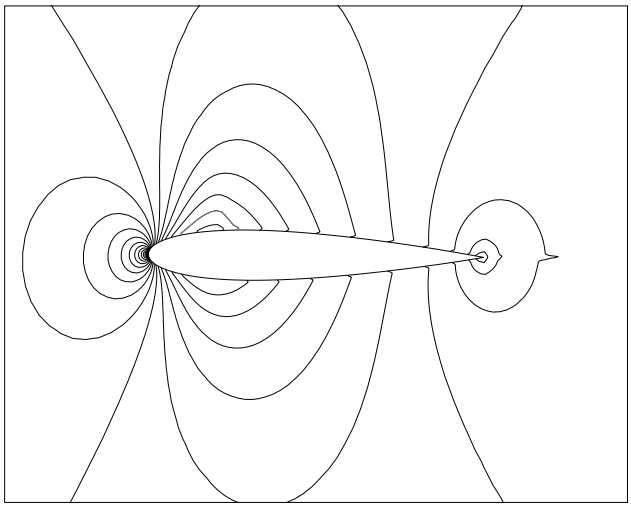

**Fig. 11a.** Unsteady Mach contours; $\phi = 0°$.

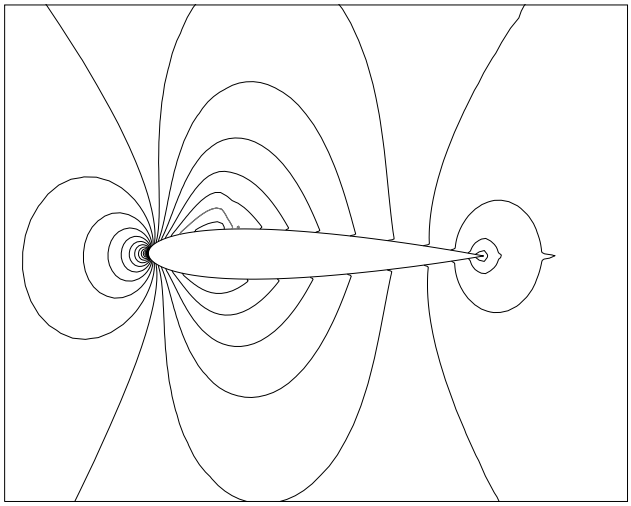

**Fig. 11b.** Unsteady Mach contours; $\phi = 30°$.

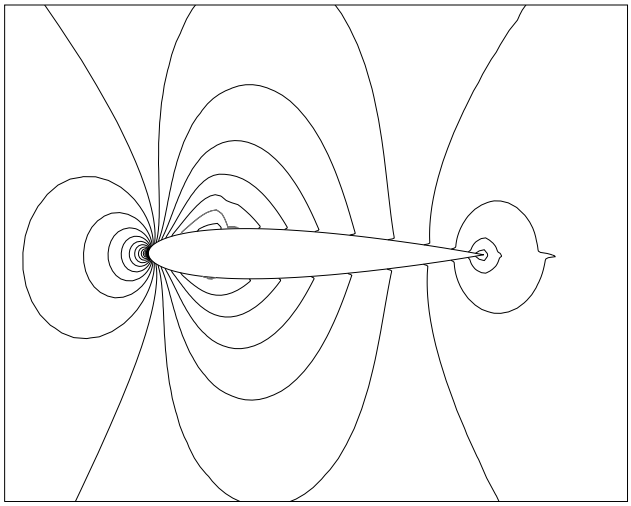

**Fig. 11c.** Unsteady Mach contours; $\phi = 60°$.

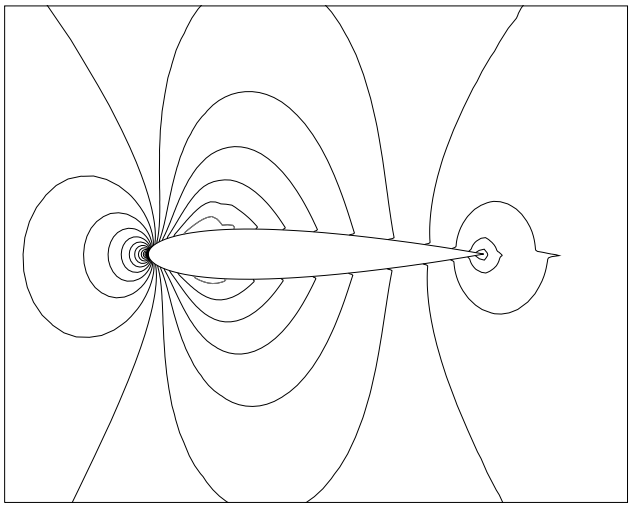

**Fig. 11d.** Unsteady Mach contours; $\phi = 90°$.

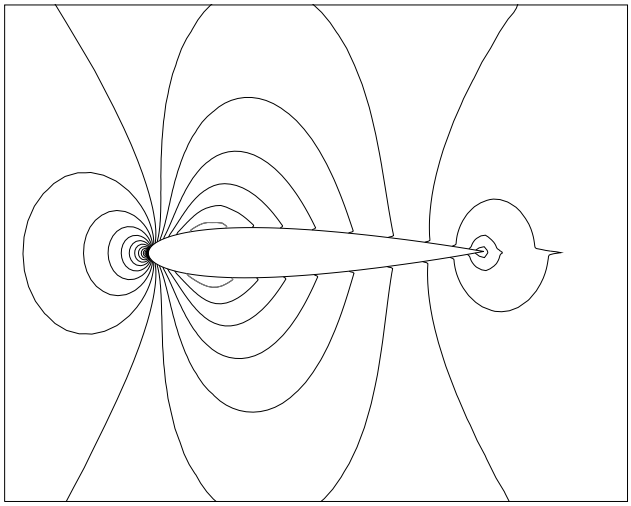

**Fig. 11e.** Unsteady Mach contours; $\phi = 120°$.

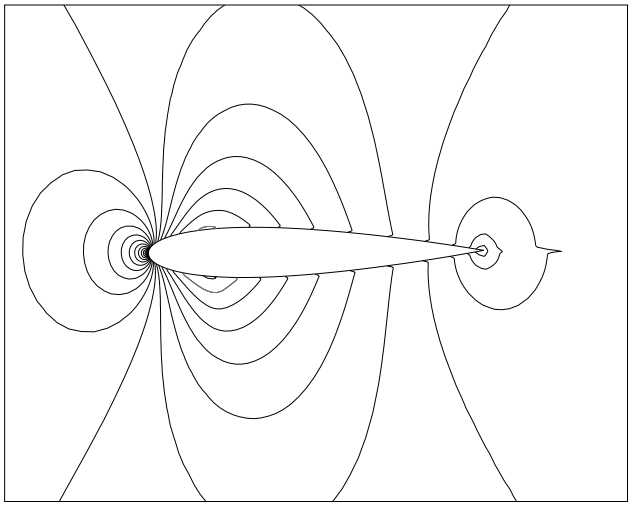

**Fig. 11f.** Unsteady Mach contours; $\phi = 150°$.

In the unsteady case, at the flutter condition ($k_\alpha = 0.359$, $k = 0.381$, $I_\alpha = 50$ and $x_p = 0$) there is a small supersonic region on either surface over part of the cycle, but no apparent shock, as shown in Fig. 11, at 30 degree intervals over half the cycle. The contour levels and sonic line are indicated as in Fig. 10.

In Fig. 12 the linear theory results from Ref. 7 (originally extracted from Ref. 25) are shown for a flat plate oscillating about its leading edge at several Mach numbers and as a function of the inertial parameter. The shift in the flutter boundaries due to increasing Mach number is similar to the thickness effect shown in Fig. 6.

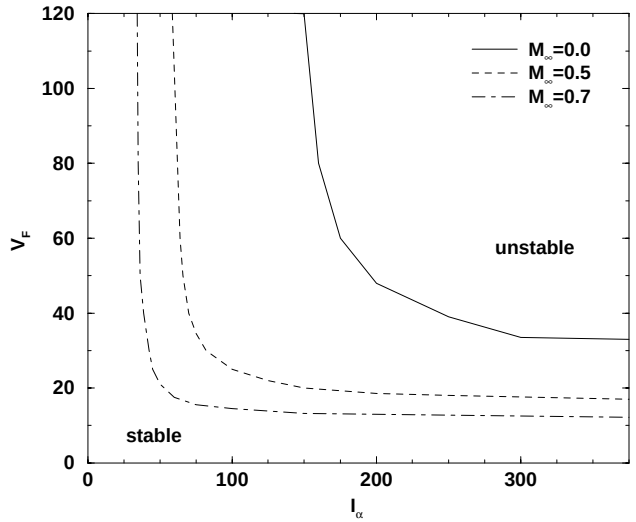


**Fig. 12.** Compressibility effect for a flat plate.

In Fig. 13 the flutter boundaries for a NACA0012 pitching about its leading edge at Mach 0 (panel code), 0.1, 0.3 and 0.5 (Euler code) are shown as a function of the inertial parameter.

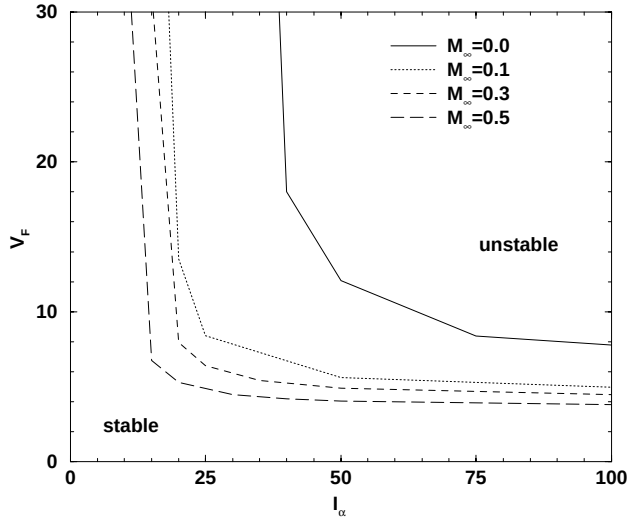


**Fig. 13.** Compressibility effect for a NACA0012.

The trend is in agreement with linear theory, but the compressible results do not appear to asymptotically approach the incompressible limit as the Mach number is reduced; a fact that warrants further investigation.

In Fig. 14 the computed untable regions for a NACA0006 and NACA0015 at Mach 0 (panel code) and Mach 0.7 (Euler code) are compared to linear theory for a range of elastic axes. It is evident that both increasing airfoil thickness and Mach number lead to significantly expanded regions of flutter instability. The flutter boundary for the NACA0015 at Mach 0.7 is roughly double that of linear theory and more than four times that predicted by incompressible linear theory.

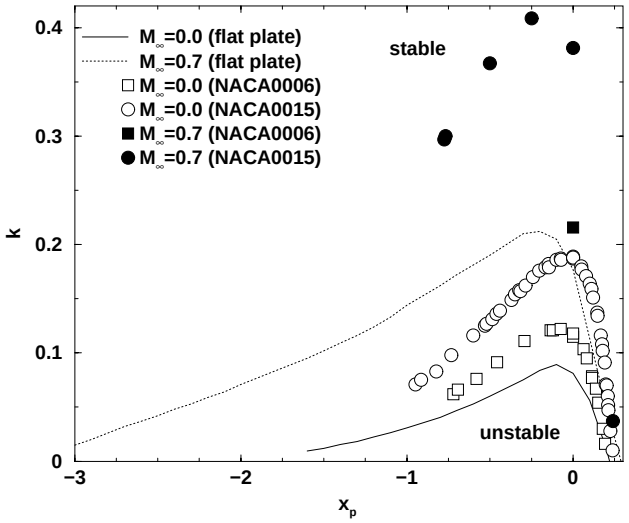


**Fig. 14.** Compressible flutter-instability regions.

## CONCLUSIONS

A two-degree-of-freedom structural model was coupled in the time-domain with an incompressible panel code and an Euler/Navier-Stokes code, and the resulting aeroelastic solvers were used to compute the unsteady motions of airfoils for the purpose of predicting airfoil flutter.

While quantitative comparisons with linear theory were not possible due to the requirement of finite airfoil thickness in the present methods, both the incompressible panel code and the compressible Euler code results provided excellent qualitative agreement with linear theory. Presented results demonstrated similar destabilizing trends for increasing airfoil thickness and increasing Mach number.

While linear theory has historically suggested that single-degree-of-freedom flutter was of only academic interest due to the unrealistically high inertial param-

eters required to achieve flutter, the panel and the Euler code predicted significantly greater regions of flutter instability than linearized (flat plate) theory. For a NACA0015 the panel code predicted reduced flutter velocities of roughly half that predicted by incompressible linear theory, and for the same airfoil at Mach 0.7 the Euler code predicted reduced flutter velocities of half that again. Furthermore, the NACA0015 airfoil at Mach 0.7 was found to flutter with an inertial parameter a full order of magnitude lower than that predicted by linear theory.

## REFERENCES


[1] Theodorsen, T., "General Theory of Aerodynamic Instability and the Mechanism of Flutter," NACA Report 496, 1935.

[2] Theodorsen, T. and Garrick, I. E., " Mechanism of Flutter," NACA Report 685, 1940.

[3] Garrick, I. E., "Propulsion of a Flapping and Oscillating Airfoil," NACA Report 567, 1936.

[4] Loewy, R. G., "A Two-Dimensional Approximation to the Unsteady Aerodynamics of Rotary Wings," **Journal of the Aeronautical Sciences**, Vol. 24, No. 2, Feb. 1957, pp. 81-106.

[5] Smilg, B., "The Instability of Pitching Oscillations of an Airfoil in Subsonic Incompressible Potential Flow," **Journal of the Aeronautical Sciences**, Vol. 16, No. 11, Nov. 1949, pp. 691-696.

[6] Runyan, H. L., "Single-degree-of-freedom Flutter Calculations for a Wing in Subsonic Potential Flow and Comparisons with an Experiment," NACA TN-2396, 1951.

[7] Bisplinghoff, R. L., Ashley, H. and Halfman, R. L., Aeroelasticity, Addison-Wesley Publishing Company, Inc., Massachusetts, 1951, pp. 617-620.

[8] Teng, N. H., "The Development of a Computer Code for the Numerical Solution of Unsteady, Inviscid and Incompressible Flow over an Airfoil," Master's Thesis, Naval Postgraduate School, Monterey, CA, June 1987.

[9] Pang, C. K., "A Computer Code for Unsteady Incompressible Flow past Two Airfoils," Aeronautical Engineer's Thesis, Naval Postgraduate School, Monterey, CA, Sept. 1988.

[10] Neace, K. S., "A Computational and Experimental Investigation of the Propulsive and Lifting Characteristics of Oscillating Airfoils and Airfoil Combinations in Incompressible Flow," Master's Thesis, Dept. of Aeronautics and Astronautics, Naval Postgraduate School, Monterey, CA, Sept. 1992.

[11] Platzer, M. F., Neace, K. S. and Pang, C. K., "Aerodynamic Analysis of Flapping Wing Propulsion," AIAA Paper No. 93-0484, Jan. 1993.

[12] Riester, P. J., "A Computational and Experimental Investigation of Incompressible Oscillatory Airfoil Flow and Flutter Problems," Master's Thesis, Naval Postgraduate School, Monterey, CA, June 1993.

[13] Turner, M., "A Computational Investigation of Wake-Induced Airfoil Flutter in Incompressible Flow and Active Flutter Control," Master's Thesis, Naval Postgraduate School, Monterey, CA, March, 1994.

[14] Jones, K. D., Dohring, C. M. and Platzer, M. F., "Wake Structures Behind Plunging Airfoils: A Comparison of Numerical and Experimental Results," AIAA Paper No. 96-0078, 1996.

[15] Jones, K. D. and Platzer, M. F., "Time-Domain Analysis of Low-Speed Airfoil Flutter," **AIAA Journal**, Vol. 34, No. 5, May 1996.

[16] Hess, J. L. and Smith, A. M. O., "Calculation of Potential Flow about Arbitrary Bodies," **Progress in Aeronautical Sciences**, Vol. 8, pp. 1-138, Pergamon Press, Oxford, 1966.

[17] Basu, B. C. and Hancock, G. J., "The Unsteady Motion of a Two-Dimensional Aerofoil in Incompressible Inviscid Flow," **Journal of Fluid Mechanics**, Vol. 87, 1978, pp. 159-168.

[18] Chakravarthy, S. R. and Osher, S., "A New Class of High Accuracy TVD Schemes for Hyperbolic Conservation Laws," AIAA Paper 85-0363, 1985.

[19] Rai, M. M. and Chakravarthy, S. R., " An Implicit Form of the Osher Upwind Scheme," **AIAA Journal**, Vol. 24, No. 5, May, 1988, pp. 735-743.

[20] Steger, J. L. and Warming, R. F., "Flux Vector Splitting of the Inviscid Gas Dynamic Equations with Applications to Finite-Difference Methods," **Journal of Computational Physics**, Vol. 40, 1981, pp. 263-293.

[21] Grohsmeyer, S. P., Ekaterinaris, J. A. and Platzer, M. F., "Numerical Investigation of the Effect of Leading Edge Geometry on Dynamic Stall of Airfoils," *AIAA 22nd Fluid Dynamics, Plasma Dynamics & Lasers Conference*, AIAA Paper No. 91-1798, June 1991.

[22] Clarkson, J. D., Ekaterinaris, J. A. and Platzer, M. F., "Computational Investigation of Airfoil Stall Flutter," presented at the *6th International Symposium on Unsteady Aerodynamics, Aeroacoustics and Aeroelasticity of Turbomachines and Propellers*, Sept., 1991.

[23] Cricelli, A. S., Ekaterinaris, J. A. and Platzer, M. F., "Unsteady Airfoil Flow Solutions on Moving Zonal Grids," *AIAA 30th Aerospace Sciences Meeting*, AIAA Paper No. 92-0543, Jan. 1992.

[24] Lambourne, N. C., "Flutter in One Degree of Freedom," Part V, Chapter 5, AGARD Manual on Aeroelasticity, General Ed. W. P. Jones, Oct. 1961.

[25] Runyan, H. T., Cunningham, H. J. and Watkins, C. E., "Theoretical Investigation of Several Types of Single Degree of Freedom Flutter," **Journal of the Aeronautical Sciences**, Vol. 19, No. 2, Feb. 1952.